Lab 2 Report: Visualizing vectors and cross-validating results

October 3, 2023

1 Introduction

We are back at XYZ Corp. working on the design of a new vertical transmitter for a long distance radio communications system. Part of the design process entails determining the net amount of power carried through three particular surfaces located near the transmitter antenna.

The analytical techniques we employed were to determine a closed-form solution to a well-posed problem followed creating by a numerical model that can be validated by that previous solution and applied to more general problems and in this case more difficult to analyze geometry.

The results of our attempts to model the power flux through the 3 surfaces resulted in a very close approximation that was validated by the closed-form solution for Surface A, and two reasonable values for Surfaces B and C. The power flux through Surface A was determined to be $20.994W$, the flux through Surface B was determined to be $2.922W$ and the flux through Surface C was determined to be $3.842W$ [Table 2]

2 Numerical Approach

The MATLAB script is approximating integration through the use of sequential sums over small subsections of each surface. The power flux through each subsection is evaluated element wise over a mesh of all subsections allowing us to approximate the area of the power flux as a rectangular surface with the dimensions of each subsection. Note: this approximation of the surface subsections as a rectangular surface is sufficient with a high enough sample rate, however if the sample rate is too low then there is a significant risk that off angle defined surfaces such as the hemisphere and cylinder would not have a constant area for each subsection.

As each power flux is calculated for each subsection of the surfaces it is both added to a combination sum of all power evaluated then summed and reported as the total surface power flux, as well as individual subsection power is assigned to a mesh indexed identically to the coordinate mesh, which allows for later plotting of the flux vector field.

For Surface A, the coordinate mesh of all subsection originally are generated in spherical coordinates, meaning that they do not need to be converted before being evaluated in the sum loops. However, Surfaces B and C are initially defined in Cartesian and Cylindrical coordinates respectively, meaning their subsections coordinates must be converted to spherical coordinates before the sums can be evaluated though our calculation process. These complex conversion algorithms introduce additional challenges where that the surface normal vectors also need conversion and are evaluated for each subsection in order to preserve the contribution of the dot product element of power flux.

The approach we took to preserving the normal maps for surfaces B and C was to create a second mesh identical size as the coordinate mesh's containing the unit normal vectors for each subsection of the surface. These meshes can then be passed through the same Cartesian-to-spherical and Cylindrical-to-Spherical conversion as the coordinate meshes. The dot product of each is evaluated for each subsection's indexed normal vector and indexed spherical coordinates, which are normalized to be unit vectors.

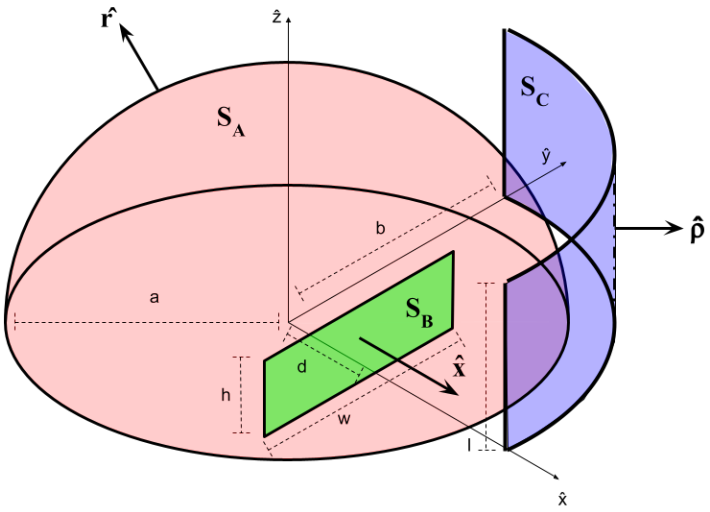

Figure 1: A rough sketch of the 3 surfaces (A,B,&C), their critical dimensions [Table 1] and normal vector components.

Model	**Surface A**	**Surface B**			**Surface C**	
A	a	d	h	w	b	l
5	3	1	0.5	2	3.5	3.5

Table 1: Provided dimensions for the various surface geometries in addition to the proportionality constant A.

3 Surface A: Hemisphere

3.1 Surface A Closed-Form Solution

Our approach for our closed-form solution for surface A consisted of using integration to determine the power generated by small subsections of our initial hemisphere. We used spherical coordinates due to the ease with our given figure and were able to apply our givens easily to this method producing us with a reliable result which we then apply to our simulation verificaion.

$$\bar{S}(r,\theta,\phi) = \hat{r}A\frac{sin^2\theta}{r^2} \tag{1}$$

$$P = \int_S \bar{S}\cdot d\bar{s} = \int_S \hat{r}A\frac{sin^2\theta}{r^2}\cdot\hat{r}ds \tag{2}$$

$$P = \int_0^{\pi/2}\int_0^{2\pi} A\,\frac{sin^2\theta}{r^2}(\hat{r}\cdot\hat{r})\,r^2 sin\theta\;d\phi d\theta = 2\pi A\int_0^{\pi/2} sin^3\theta\;d\phi d\theta \tag{3}$$

$$P = 2\pi A\left(\frac{1}{12}(cos(3\theta)-9cos\theta)\right)\Big|_{\theta=0}^{\pi/2} \tag{4}$$

$$P = \frac{4\pi A}{3}\Big|_{A=5} = \frac{20\pi}{3} = 20.944 \tag{5}$$

3.2 Simulated Power Flux

The final value for the power flux through Surface A was determined to be $20.935W$, which was calculated as the sum from 2000 surface subdivisions. This value is validated by our closed-form solution with an error of 0.04% and which would presumably converge to the true value if it were possible to simulate infinite subdivisions. [Figure 2]

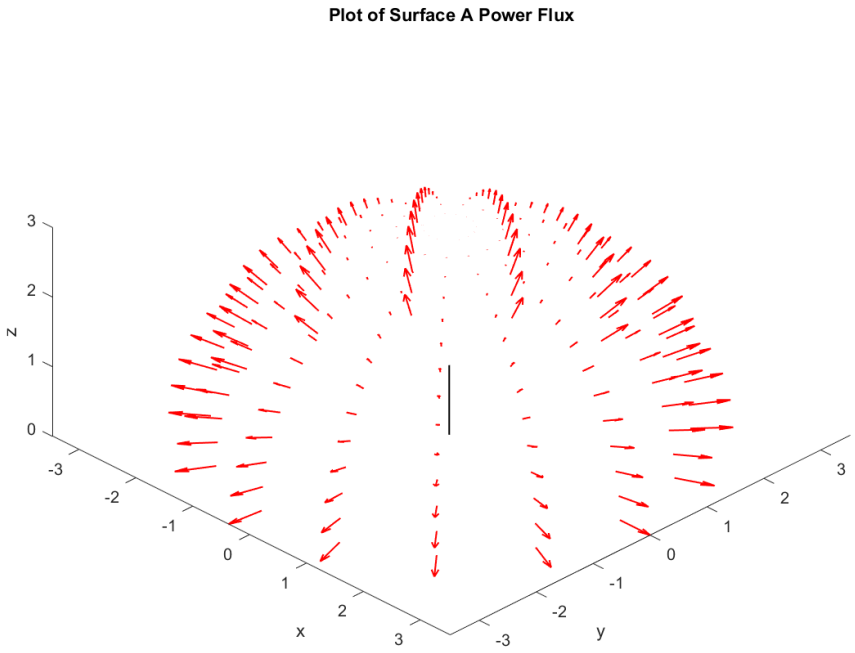

Figure 2: A 3D plot of the power flux vector field for surface A with 15x15 surface subdivisions. The individual vector magnitudes show how the power flux is radial to the origin and attenuates toward the top of the hemispheres, where the $sin^3\theta$ is minimized. Note: a black line of extending from $z \subset [0, 1]$ is included in the plot to represent the signal source

4 Surface B: Rectangular Plane

A closed-form solution for this surface was not attempted, primarily due to the anticipated complexity of evaluating the power integral with references to two distinct coordinate systems. Throughout our design process we encountered errors with of conversion from Rectangular-to-Spherical Coordinates. During our initial conversions we detected that our divisions were not producing correct due to our conversion formula and our attention to unit vectors. After closely examining our formula and correcting syntactical errors, our conversion and output flux resulted in reasonable values. Other than these initial setbacks the numerical analysis of Surface B was accomplished by first defining the surface in Cartesian coordinates followed by conversion into spherical coordinates. The normal map was included in the evaluation only reflecting the $\hat{x}$ direction. The power flux was then evaluated over the subsections of the surface and summed.

4.1 Simulated Power Flux

The final value for the power flux through Surface B was determined to be $2.922W$, which was calculated as the sum from 2000 surface subdivisions. This value cannot be validated by a closed-form solution to determine our model error, however we can perform a simple check on the magnitude of this power flux as a proportion of the 'maximum' calculated for Surface A. The flux through surface B accounts for only 13.9% of the power captured through surface A which is reasonable considering Surface B's proximity to the antenna source and angular size with respect to the origin. [Figure 3]

5 Surface C: Cylinder Wall Section

A closed-form solution for this surface was not attempted, primarily due to the anticipated complexity of evaluating the power integral with references to two distinct coordinate systems. The numerical

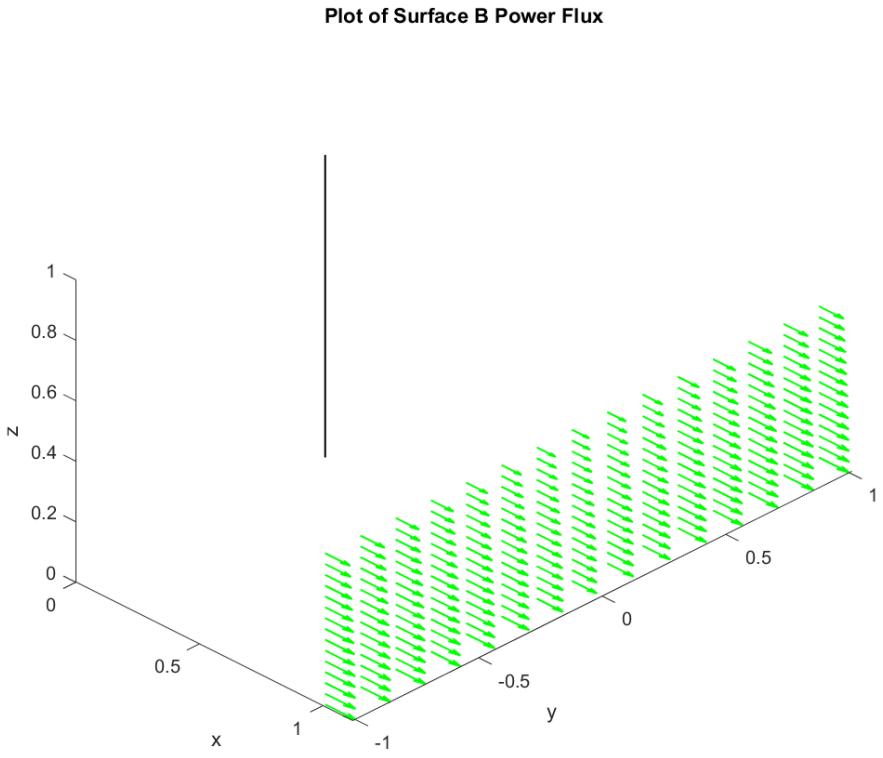

Figure 3: A 3D plot of the power flux vector field for surface B with 15x15 surface subdivisions. The individual vector magnitudes show how the power flux through the surface is maximized at the base of the rectangle and extend normal to the planar surface geometry. Note: a black line of extending from $z \subset [0, 1]$ is included in the plot to represent the signal source

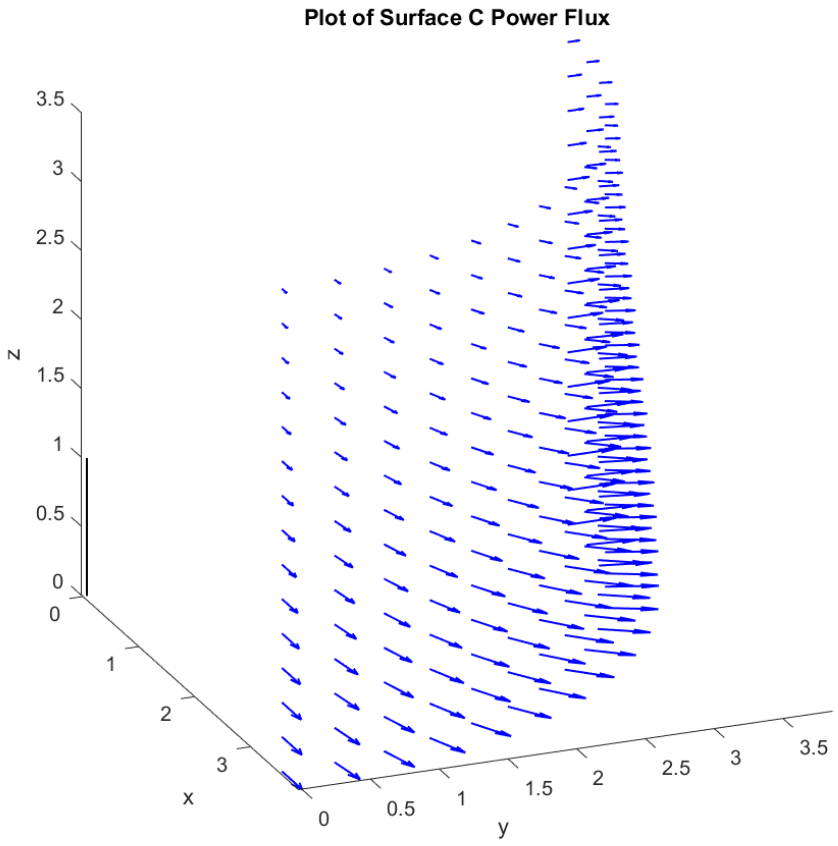

Figure 4: A 3D plot of the power flux vector field for surface C with 15x15 surface subdivisions. The individual vector magnitudes show how the power flux through the surface is once again maximized at its base and extend normal to the cylinder surface geometry. Note: a black line of extending from $z \subset [0, 1]$ is included in the plot to represent the signal source

analysis of Surface C was undertaken in a similar manner to Surface B, where first the cylindrical coordinates defining the surface were converted into spherical coordinates, along with the normal map only reflecting the $\hat{\rho}$ direction. The power flux was then evaluated over the subsections of the surface and summed.

5.1 Simulated Power Flux

The final value for the power flux through Surface B was determined to be $3.842W$, which was calculated as the sum from 2000 surface subdivisions. This value again cannot be validated by a closed-form solution to determine our model error, but can evaluate the flux with respect to Surface A. The flux through surface B accounts for only 18.3% of the power captured through surface A which is reasonable considering the its overall distance from the antenna source and angular size with respect to the origin. [Figure 4]

6 Comparison of Numerical and Analytical Results

Referring to Table 2, one can see the discrepancy between our analytical solution and simulated solution. Throughout our testing, possible sources of error included choices for our mesh component sizes which could lead to larger or smaller discrepancies in our total power calculations. Also we calculated that our method for conversions creates a small area for errors due to the uncertainty of

	Surface A	Surface B	Surface C
Analytical Solution [W]	20.994	—	—
Simulated Solution [W]	20.935	2.922	3.842

Table 2: Power flux through each surface by evaluation method. An analytical solution was attempted for the spherical case of Surface A due to the ease of evaluating it exclusively in spherical coordinates. An analytical solution of B and C are potentially possible, but any more complex geometry would necessarily have to be simulation.

our estimation in conversions using the finite sum approach. Along with those, for surfaces B and C, we did not have a analytical calculation to base our results off, in turn, preventing us from validation our simulations accuracy.

7 Conclusions and Implications

Throughout our experiment, we determined the use of our simulation to create a fairly accurate conversion algorithm demonstrating how we can apply coordinate conversions to non-traditional shapes to produce a flux output. Referencing our analytical and simulation solutions we notice that we are able to verify our surface A solution but not surfaces B and C. As we were able to apply our analytical solutions to create the conversions method for the later, we are able to calculate the power flux through the finite sum method for non-traditional shapes. Overall, the verification of surface A gave us a benchmark for our accuracy on surface B and C allowing for some confidence in our simulation which can now be applied to alternate figures and problems. Our application of these methods proved to be a viable solution to determining the net power carried through three particular surfaces located near this transmitters antenna and is deemed a relative success according to our analytical and simulation comparisons.

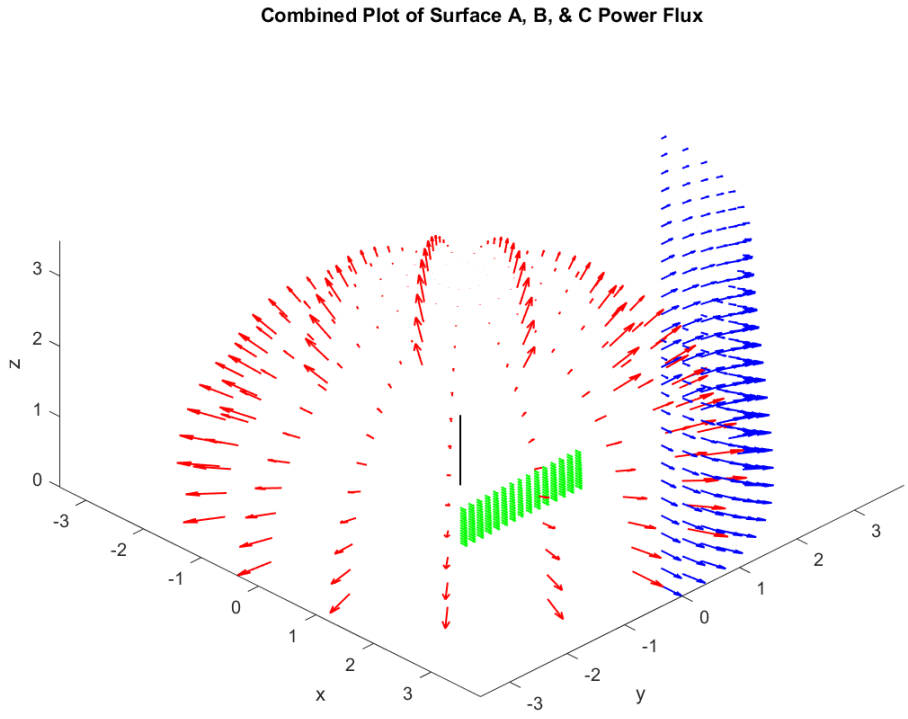

Figure 5: A 3D plot of power flux through all 3 surfaces. The individual vector magnitudes show how the power flux through the surface is once again maximized at its base. Note: a black line of extending from $z \subset [0, 1]$ is included in the plot to represent the signal source